Journal of Solid State Chemistry 181 (2008) 3344–3351

Contents lists available at ScienceDirect

Journal of Solid State Chemistry

journal homepage: www.elsevier.com/locate/jssc

Synthesis, phase transition and photoluminescence studies on Eu^{3+}-substituted double perovskites—A novel orange-red phosphor for solid-state lighting

V. Sivakumar *,[1], U.V. Varadaraju *

Materials Science Research Centre and Department of Chemistry, Indian Institute of Technology—Madras, Chennai 600 036, India

ARTICLE INFO

Article history:
Received 18 June 2008
Received in revised form
12 August 2008
Accepted 24 August 2008
Available online 1 October 2008

Keywords:
Double perovskite
Orange-red phosphor
White light-emitting diode
Photoluminescence

ABSTRACT

Photoluminescence studies on Eu^{3+}-doped double perovskites with the formula A_2CaWO_6 (A = Sr, Ba) revealed that the forced electric dipole (ED) transition is present when Eu^{3+} is substituted at the non-centrosymmetric Sr-site vis-a-vis substitution at the centrosymmetric Ca-site shows both ED and magnetic dipole (MD) transition. A series of novel orange-red-emitting phosphor compositions $Sr_{1.9-x}Ba_xEu_{0.05}Li_{0.05}CaWO_6$ ($x = 0$–1.9) have also been synthesized and characterized by powder X-ray diffraction (XRD), diffuse reflectance spectroscopy (DRS) and photoluminescence. XRD results reveal a phase transition from monoclinic to pseudo-cubic structure for $x \leqslant 0.2$. All the compositions show broad charge transfer band and orange-red (MD and ED) emission. However, the relative intensity of the MD and ED depends on the Ba content present in the host lattice. Select compositions in this system of compounds could find potential application as orange-red phosphors for white light generation using blue/near-UV GaN-based light-emitting diodes (LEDs).

1. Introduction

Phosphor research is immensely important due to their emerging technology such as lamp, plasma display panels (PDPs), field emission displays (FEDs) and solid-state lighting (SSL). White light based on light-emitting diodes (LEDs) is already begun to replace the traditional incandescent lamps and expected to replace fluorescent lamps in the near future. Now it is consider being a new generation of lighting owing to their high efficiency, reliability and low energy consumption. The first white LED has been fabricated using blue LED with yellow phosphor YAG:Ce^{3+} [1]. In order to improve the efficiency of the phosphor, crystal chemical substitutions have been carried out in the phosphor host lattice YAG:Ce^{3+} ($(Y_{1-a}Gd_a)_3(Al_{1-b}Ga_b)_5O_{12}$:$Ce^{3+}$). However, the spectral composition of the light created by the conventional two-band white LED (blue LED+yellow phosphor) differs from that of natural white light due to halo effect of blue/yellow color separation and poor color rendering index (CRI) caused by the lack of red emission [2]. The other approach to obtain white light is to combine UV LED/laser diode with blue, green and red (BGR) phosphors [3]. High performance white LEDs have been fabricated by using NUV LED with blue, green, yellow, orange and red phosphors (BGYOR), which are based on SrS- and ZnS-based long wavelength phosphors [4]. Most of the red phosphors that are used for LED application are sulfide-based phosphors (CaS:Eu^{2+}, SrY_2S_4:Eu^{2+}, Y_2O_2S:Eu^{3+} and ZnCdS:Cu, Al). However, there are certain disadvantages in using sulfide-based materials; the efficiency of the Y_2O_2S:Eu^{3+} red phosphor is less than that of the green and blue phosphors. These sulfide-based phosphors are chemically unstable and the life time of the materials is inadequate under extended UV irradiation. We have reported Eu^{3+}-substituted phosphors containing WO_4 and MoO_4 tetrahedra with scheelite-related structures [5,6]. Here the efficiency of charge transfer (CT) band (due to MoO_4/WO_4 tetrahedra) is not good enough to give high emission intensity for near-UV excitation. Recently, we have explored the possibility of Eu^{3+}-doped double perovskite structure with MoO_6 octahedra as potential candidate for orange-red-emitting phosphor for white LEDs [7,8].

In the present study, Eu^{3+}-substituted (A- and B-sites) double perovskite with formula A_2CaWO_6 (A = Sr and Ba) has been synthesized and its photoluminescence properties are studied. Further we also made a series of Ba-substituted compositions ($Sr_{1.9-x}Ba_xEu_{0.05}Li_{0.05}CaWO_6$ ($x = 0$–1.9)) and investigated their phase formation/transition and optical properties, and compared

* Corresponding authors.
E-mail addresses: vai.sivakumar@gmail.com, sivakumar@kaist.ac.kr (V. Sivakumar), varada@iitm.ac.in (U.V. Varadaraju).
[1] Present address: Display Materials Lab, Department of Materials Science and Engineering, Korea Advanced Institute of Science and Technology, Deajeon 305-701, Republic of Korea. Fax: +82 42 869 3310.

0022-4596/$ - see front matter © 2008 Elsevier Inc. All rights reserved.
doi:10.1016/j.jssc.2008.08.030

their emission intensities with the commercial red phosphor ($Y_2O_2S:Eu^{3+}$, Nichia).

2. Experimental

2.1. Synthesis and characterization

Phases of nominal composition A_2CaWO_6 (A = Sr and Ba) were synthesized by conventional high-temperature solid-state reaction. Stoichiometric amounts of $SrCO_3$ (Cerac, 99.995%), $BaCO_3$ (Alfa Aesar, 99.5%), $CaCO_3$ (Cerac, 99.995%), Eu_2O_3 (Indian Rare earths, 99.9%), Li_2CO_3 (Merck, 99.9%) and WO_3 (Alfa, 99%) were intimately ground and heated in air at 600 °C for 12 h to decompose the carbonates. The powder samples were ground again and heated in air at 900 °C for 24 h. The obtained product was heated at 1100 °C for 24 h with intermittent grinding.

Phase purity was identified by powder X-ray diffraction (XRD) using Cu-$K\alpha_1$ radiation (P3000-Rich Seifert). Diffraction patterns were taken over the 2θ range 10–70°. Lattice parameters were calculated using least-square method (AUTOX programme). The diffuse reflectance spectra were recorded using a UV–vis diffuse reflectance spectrophotometer with 150 mm integrating sphere (Jasco spectrophotometer). $BaSO_4$ was used as a reference for 100% reflectance. Reflectance data were collected and converted to absorbance. The excitation (PLE) and emission (PL) spectra were recorded using Spectrofluorolog (JOBINYVON). All the measurements were performed at room temperature.

3. Results and discussion

3.1. Phase formation and crystal structure of A_2CaWO_6 (A = Sr and Ba)

The powder XRD pattern of Sr_2CaWO_6 as well as those of compositions wherein Eu is substituted at the A- and B-sites is shown in Fig. 1. It is well-known that hexavalent Mo and W are stabilized not in the primitive ABO_3 perovskite structure but in the ordered double perovskite structure, $A_2^{II}B^{II}B^{VI}O_6$ ($A_2BB'O_6$), in which A^{II} is an alkaline earth ion, B^{II}, a divalent metal ion such as Mg, Ca, Ni and Cu, and B^{VI}, a hexavalent Mo or W ion. It has been reported that if the charge difference between B and B' is four, the compounds adopt an ordered perovskite structure with the rock-salt arrangement of B and B' ions [9]. Sr_2CaWO_6 crystallizes in orthorhombic structure with space group $Pmm2$ and the calculated lattice parameters are $a = 8.184(2)$, $b = 5.839(2)$ and $c = 5.761(2)$ [10]. Recent crystallographic studies show that Sr_2CaWO_6 crystallizes in monoclinic structure with space group $P21/n$ [11,12]. In Sr_2CaWO_6 structure, A-site is exclusively occupied by Sr^{2+} ions and B-site is occupied by the Ca^{2+} and W^{6+} ions and ordering has been observed in the B-site cations [7]. From the XRD patterns, splitting of some diffraction peaks was observed and all the peaks could be indexed based on monoclinic structure with space group $P21/n$. The calculated lattice parameters are tabulated in Table 1.

Fig. 2 shows X-ray powder diffraction patterns of Eu-substituted (A- and B-sites) and parent (Ba_2CaWO_6) phase. It has been reported that the Ba_2CaWO_6 crystallizes in pseudo-cubic structure with space group Fm-3m and the lattice parameter is $a = 8.375(2)$ [10]. The crystal structure of Ba_2CaWO_6 is shown in Fig. 3. Ba^{2+} (A-site) ions are coordinated to 12 oxygen atoms and Ca^{2+}/W^{6+} are coordinated to 6 oxygen atoms and the Ca^{2+} and W^{6+} ions are ordered in the B-site [13]. Ordering between the B and B' ions is quite common for cubic perovskites of the type $A_2BB'O_6$, if the charge difference between B and B' ions is $\geqslant 4$ [14]. The positions of the ordered ions are like those of cations and anions in the rock-salt structure. All the peaks could be indexed based on pseudo-cubic structure with space group Fm-3m. The calculated lattice parameters for phases with Eu^{3+}-substituted at A- and

Table 1
Calculated lattice parameters for A- and B-site Eu-substituted A_2CaWO_6 (A = Sr and Ba) with parent phases

Compound	Lattice parameters			β (deg)
	a (Å)	b (Å)	c (Å)	
Sr_2CaWO_6	8.323(2)	5.797(7)	5.925(9)	91.19
$Sr_{1.9}Eu_{0.05}Li_{0.05}CaWO_6$	8.315(8)	5.786(7)	5.922(7)	91.26
$Sr_2Ca_{0.9}Eu_{0.05}Li_{0.05}WO_6$	8.295(6)	5.793(4)	5.916(7)	91.10
Ba_2CaWO_6	8.377(2)	–	–	–
$Ba_{1.9}Eu_{0.05}Li_{0.05}CaWO_6$	8.375(2)	–	–	–
$Ba_2Ca_{0.9}Eu_{0.05}Li_{0.05}WO_6$	8.374(2)	–	–	–

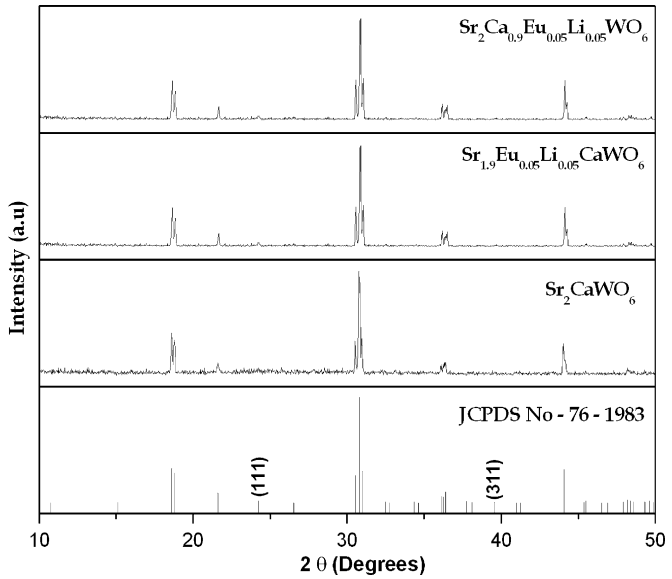

Fig. 1. Powder X-ray diffraction patterns of Sr_2CaWO_6 and Eu^{3+}-substituted phases.

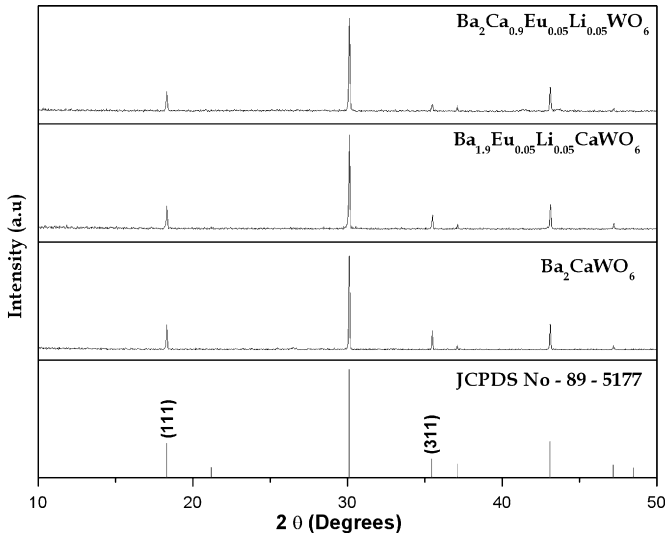

Fig. 2. Powder X-ray diffraction patterns of Ba_2CaMoO_6 and Eu^{3+}-substituted phases.

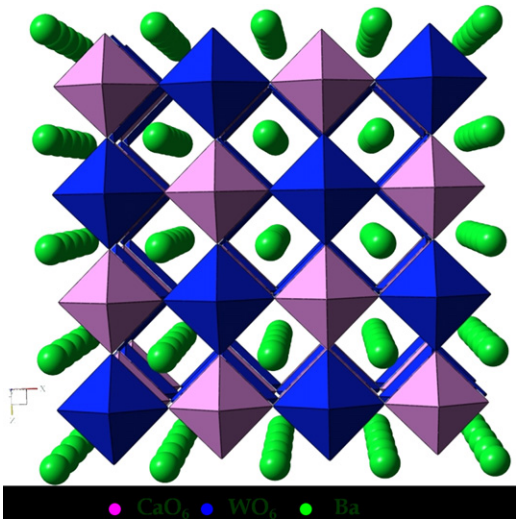

Fig. 3. Crystal structure of Ba_2CaWO_6.

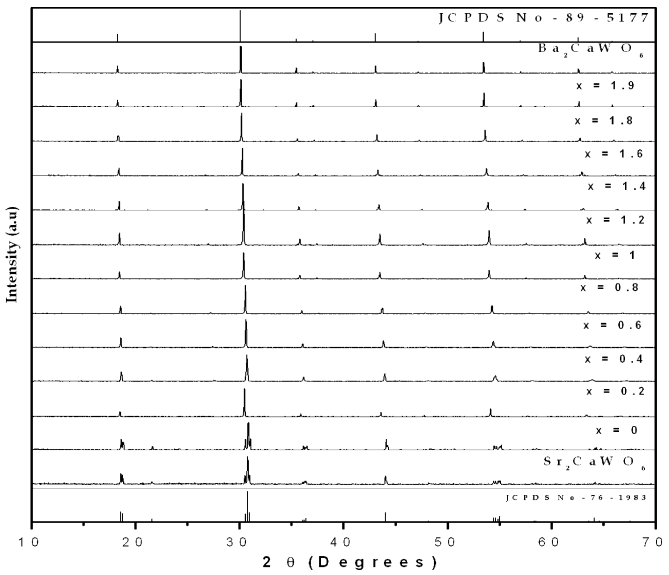

Fig. 4. Powder X-ray diffraction patterns of $Sr_{1.9-x}Ba_xEu_{0.05}Li_{0.05}CaWO_6$ ($x = 0.2$–1.9, in steps of 0.2) with parent compounds.

B-sites along with those of parent phases are tabulated in Table 1. The appearance of superlattice lines (111), (311) and (511) evidences the rock-salt ordering of Ca^{2+} and W^{6+} (Figs. 1 and 2).

XRD patterns of $Sr_{1.9-x}Ba_xEu_{0.05}Li_{0.05}CaWO_6$ ($x = 0$–1.9, in steps of 0.2) are shown in Fig. 4. In the $Sr_{1.9-x}Ba_xEu_{0.05}Li_{0.05}CaWO_6$ ($x = 0$–1.9, in steps of 0.2) system, for $x \leqslant 0.2$ all the compositions crystallize in monoclinic structure and on further increase of *x*, the system undergoes a compositionally induced phase transition from monoclinic to pseudo-cubic structure. No impurity line was found in the XRD patterns clearly indicating that the compounds formed are single phase and Eu^{3+} incorporation has been achieved. The calculated lattice parameters for all compositions are tabulated in Table 2. Linear variation is observed for '*a*' lattice parameter with increasing Ba content in the host lattice. Due to the large ionic size [15] difference between Ba^{2+} and Li^+/Eu^{3+}, some of the Li^+/Eu^{3+} ions can occupy the Ca^{2+} (*B*-site) also for higher *x* values [7,8].

Table 2
Lattice parameters of $Sr_{1.9-x}Ba_xEu_{0.05}Li_{0.05}CaWO_6$ ($x = 0$–1.9 in steps of 0.2)

Compositions	*a* (Å)	*b* (Å)	*c* (Å)	*β* (deg)
0	8.315(8)	5.786(7)	5.922(7)	91.26
0.2	8.293(2)	–	–	–
0.4	8.228(2)	–	–	–
0.6	8.253(2)	–	–	–
0.8	8.274(2)	–	–	–
1	8.295(2)	–	–	–
1.2	8.314(2)	–	–	–
1.4	8.334(2)	–	–	–
1.6	8.348(2)	–	–	–
1.8	8.368(2)	–	–	–
1.9	8.375(2)	–	–	–

3.2. Diffuse reflectance spectroscopy (DRS)

Fig. 5 shows the DRS spectra of parent and Eu^{3+}-doped Sr_2CaWO_6 and Ba_2CaWO_6 phases. Broad absorption band is observed for all compositions and this band is due to CT transition from oxygen to tungsten (O→W). In other words, electronic transition from valence band (primarily oxygen 2*p* non-bonding character) to conduction band (arises from the p^* interaction between the tungsten metal ion t_{2g} orbital and oxygen). From the DRS spectra the band gap is found to be 3.2 eV and this value matches well with the reported value [16]. The DRS spectra of A_2CaWO_6 (A = Sr and Ba) and selected compositions of $Sr_{1.9-x}Ba_xEu_{0.05}Li_{0.05}CaWO_6$ ($x = 0$–1.9, in steps of 0.2) are shown in Fig. 6. All compositions show broad absorption band ranging from 200 to 400 nm peaking at ~300 nm. The broad absorption band is assigned to CT transition of the WO_6 octahedral moiety.

3.3. Luminescence of Sr_2CaWO_6:Eu^3

The excitation spectrum of *A*-site Eu^{3+}-substituted Sr_2CaWO_6 with different monitoring wavelengths (596/615 nm) is shown in Fig. 7. The spectrum contains broad absorption band with peak maximum at ~330 nm and this band is due to oxygen to tungsten CT transition. In addition, the characteristic Eu^{3+} excitation lines are also observed in the spectrum. The relative intensity of CT band and $^5L_6$–$^7F_0$ line is found to be same. However, the intensities of $^7F_0$–$^5D_2$ and $^7F_1$–$^5D_1$ lines are found to be high when the monitoring wavelength is 615 nm. The emission of *A*-site Eu^{3+}-substituted Sr_2CaWO_6 is shown in Fig. 7. The spectrum contains sharp lines at 615 and 596 nm which are due to electric dipole (ED) and magnetic dipole (MD) transitions of Eu^{3+} ion. Generally the Eu^{3+} emission lines are hypersensitive, i.e., they are highly sensitive to the crystal chemical environment [17]. ED transition is dominant when Eu^{3+} occupies non-centrosymmetric site in the lattice [18]. In the present study, the relative intensity of ED transition is found to be high. Since Sr_2CaWO_6 crystallizes in distorted double perovskite structure (monoclinic, due to tilting of the octahedra), the surroundings of the Eu^{3+} ion do not have exact inversion symmetry. Indeed, the splitting of the lines indicates a symmetry lower than cubic, C_2, for Eu^{3+} in Sr-site (Sr_2CaWO_6). The expected number of lines for $^5D_0$–$^7F_1$ transition is 3 and for $^5D_0$–$^7F_2$ is 4. However, the emission spectrum shows broadness in the emission lines with marginal splitting.

3.4. Luminescence of B-site Eu^{3+}-substituted Sr_2CaWO_6

The excitation spectrum of Eu^{3+}-substituted (*B*-site) Sr_2CaWO_6 is shown in Fig. 8. The spectrum shows both sharp excitation lines (due to Eu^{3+}) and broad CT band (due to WO_6 octahedra). The relative intensity of CT band is found to be high when the

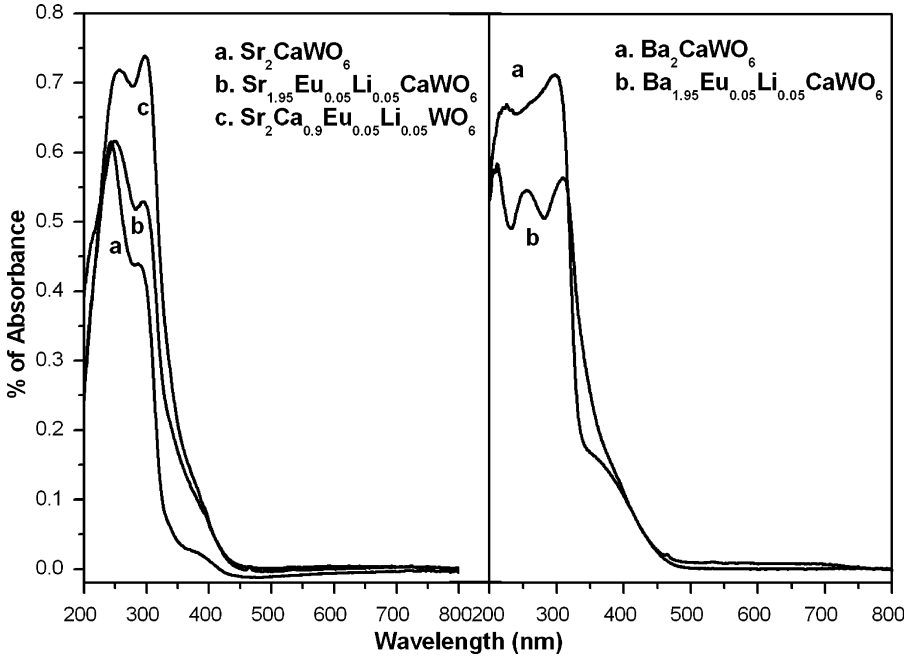

Fig. 5. DRS spectra of Eu^{3+}-substituted Sr_2CaWO_6 and Ba_2CaWO_6 with parent compound.

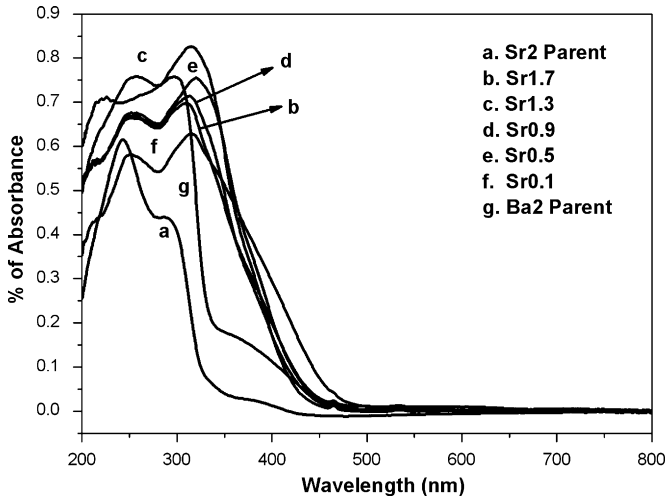

Fig. 6. DRS spectra of $Sr_{1.9-x}Ba_xEu_{0.05}Li_{0.05}CaWO_6$ ($x = 0$–1.9, in steps of 0.2).

monitoring wavelength is 596 nm. This clearly indicates that the energy transfer from absorbing group (WO_6) to Eu^{3+} is facile [7] when the Eu^{3+} ion is present in the *B*-site rather than *A*-site in the presently studied phases.

Fig. 8 shows the emission spectrum of Eu^{3+}-substituted (*B*-site) Sr_2CaWO_6. The spectrum shows both ED and MD transitions. However, the relative intensity is found to be different. The intensity of MD transition is high when compared to that of ED transition. In this structure, Ca-site (*B*-site) is octahedral with site symmetry O_h. The MD transition is not split as is to be expected for symmetry group O_h. Two lines are expected for ED transition, since the $^5D_0$ levels are degenerate and $^7F_2$ levels are split into two non-degenerate levels by crystal field symmetry of O_h. However, more than 2 lines (6 lines) were found in the emission spectrum. These lines are due to simultaneous excitation of non-centrosymmetric vibrational modes of the surroundings of the rare-earth ion, i.e., vibronic transitions. Similar observation has

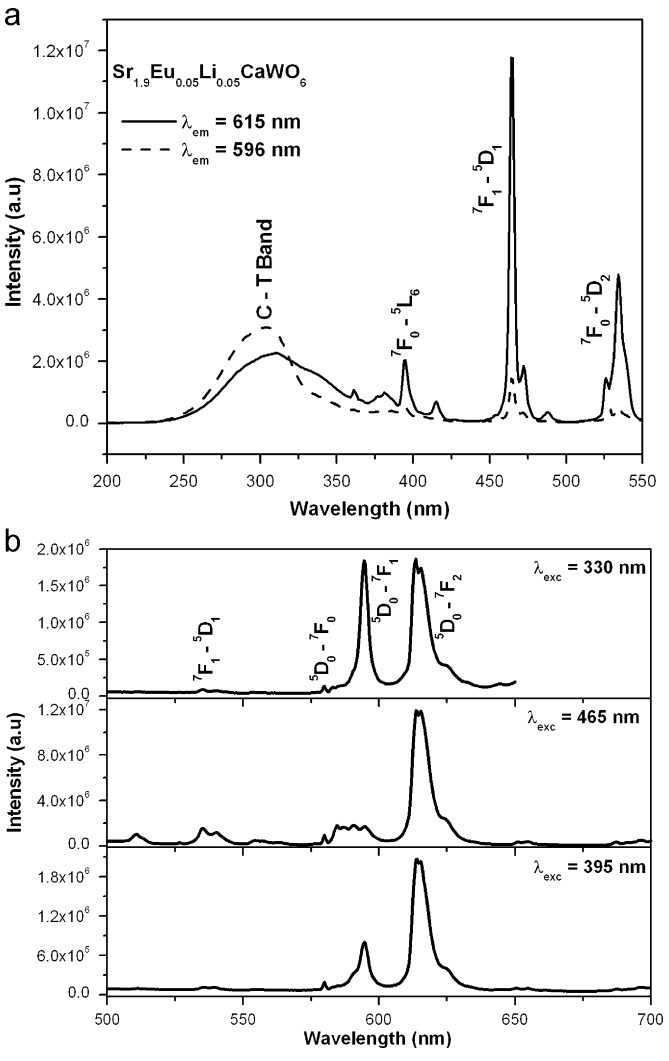

Fig. 7. PL excitation and emission spectra of $Sr_{1.9}Eu_{0.05}Li_{0.05}CaWO_6$.

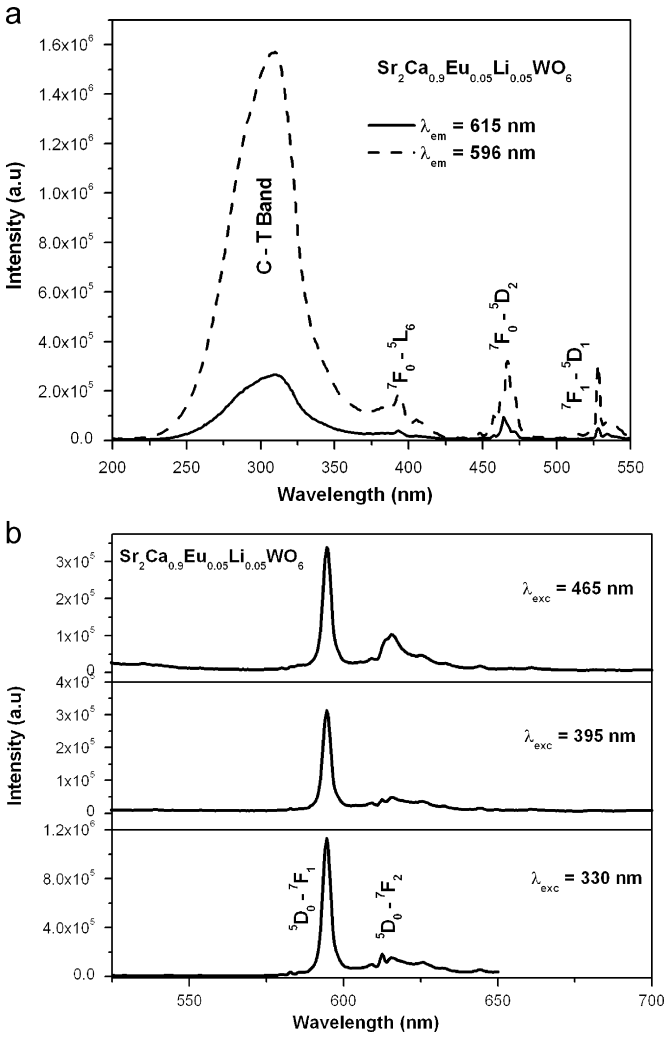

Fig. 8. PL excitation and emission spectra of $Sr_2Ca_{0.9}Eu_{0.05}Li_{0.05}WO_6$.

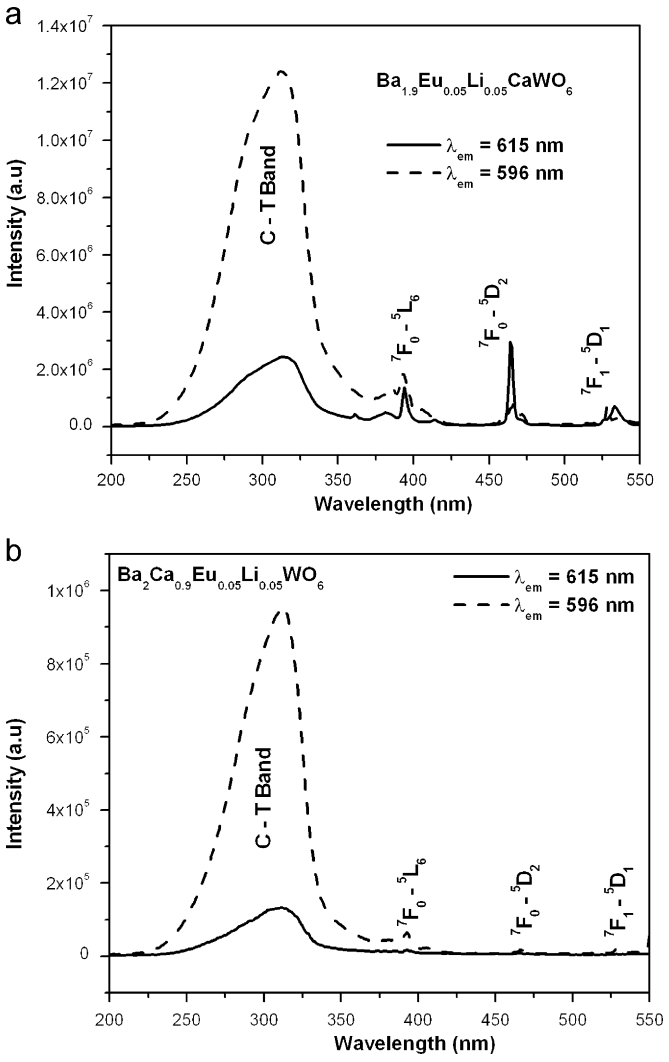

Fig. 9. PL excitation spectra of $Ba_{1.9}Eu_{0.05}Li_{0.05}CaWO_6$ and $Ba_2Ca_{0.9}Eu_{0.05}Li_{0.05}WO_6$.

been made in perovskite and double perovskite ($SrTiO_3$ and Ba_2GdWO_6) compounds [19,20]. Whatever may be the excitation wavelength, the MD transition is observed; however, the relative intensity of this line is found to be high when the excitation wavelength is CT band (330 nm). This clearly indicates that the energy transfer from absorbing group WO_6 to Eu^{3+} is very facile (Fig. 8).

3.5. Eu^{3+} luminescence in Ba_2CaWO_6

The excitation spectra of Eu^{3+}-substituted (*A*- and *B*-sites) Ba_2CaWO_6 are shown in Fig. 9. The spectra contain absorption band due to WO_6 octahedra and additional sharp lines (due to Eu^{3+}). The relative intensity of the broad band and sharp lines depends on the emission wavelength monitored. If the monitoring wavelength is 596 nm (dotted line) the broad band having high intensity rather than sharp lines, whereas the reverse is true for 615 nm monitoring wavelength (thick line) for Eu^{3+} in the *A*-site. In the case of *B*-site-substituted phases only CT band intensity is found to be high, whatever may be the monitoring wavelength (596 or 615 nm). Fig. 10 shows the emission spectra of Eu^{3+}-substituted (*A*- and *B*-sites) Ba_2CaWO_6. All compositions show ED and MD transition. However, the relative intensity of MD transition is found to be high for CT band and 394 nm excitation. This clearly indicates that the Eu^{3+} occupies centrosymmetric site in the presently studied phases. As mentioned earlier, Ba_2CaWO_6 crystallizes in pseudo-cubic structure. Hence, there is no distortion in *A*- and *B*-sites in double perovskite structure. However, the relative intensity of ED transition is found to be high for 465 nm excitation (Fig. 10).

3.6. Luminescence of $Sr_{1.9-x}Ba_xEu_{0.05}Li_{0.05}CaWO_6$ ($x = 0$–1.9, in steps of 0.2)

The excitation spectra of select compositions $Sr_{1.9-x}Ba_xEu_{0.05}Li_{0.05}CaWO_6$ ($x = 0$–1.9, in steps of 0.2) are shown in Figs. 11 and 12. A broad absorption band is observed and this is due to CT transitions of oxygen to tungsten in WO_6 octahedra [21]. These CT bands are much stronger compared to the same when MoO_4/WO_4 tetrahedra are present as in scheelite structures for NUV excitation. The photoluminescence studies on $AgGd_{0.95}Eu_{0.05}(WO_4)_{2-x}(MoO_4)_x$ ($x = 0$–2, in steps of 0.25) have shown that in the excitation spectra, the CT band is more intense for tungstates (monoclinic) compared to molybdates (tetragonal), because tungsten is coordinated with oxygen in octahedral environment whereas molybdenum is coordinated with oxygen in tetrahedral environment for NUV excitation [5]. In the present study, additional peaks are observed, which are due to *f*–*f* electronic transitions of Eu^{3+} ion. The intensity of CT band and that of *f*–*f* transitions in the excitation spectrum depends on the emission wavelength monitored (596 or 615 nm; Figs. 11 and 12). For the

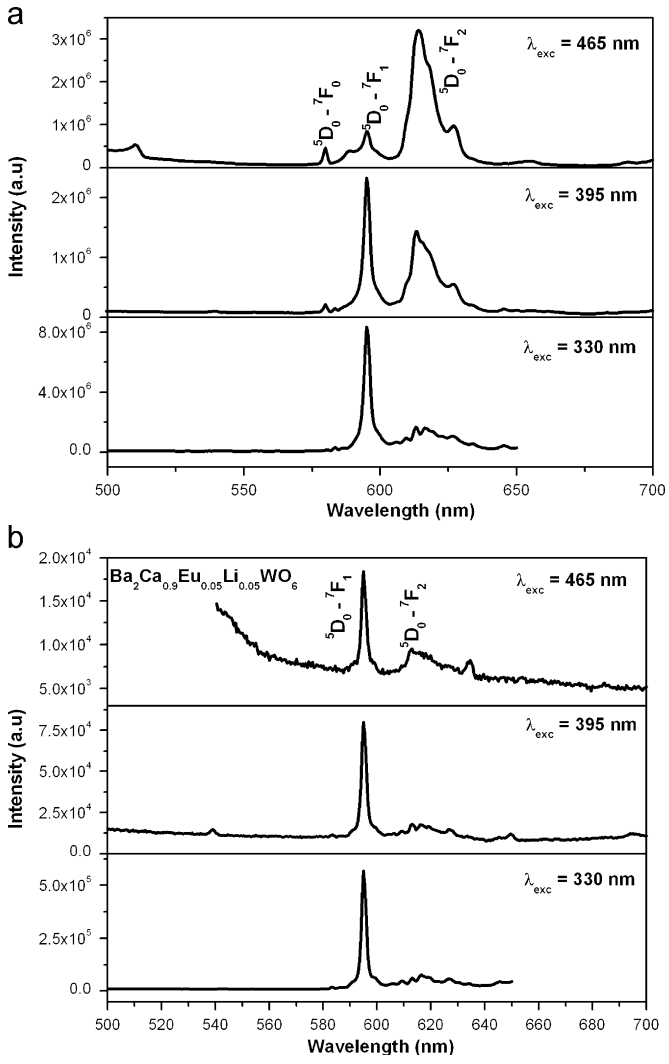

Fig. 10. PL emission spectra of $Ba_{1.9}Eu_{0.05}Li_{0.05}CaWO_6$ and $Ba_2Ca_{0.9}Eu_{0.05}Li_{0.05}WO_6$.

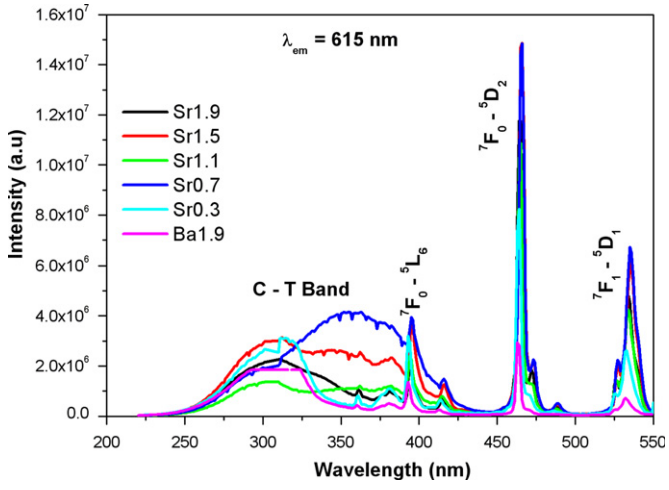

Fig. 11. PL excitation spectra of select compositions $Sr_{1.9-x}Ba_xEu_{0.05}Li_{0.05}CaWO_6$ ($x = 0$–1.9; $\lambda_{em} = 615$ nm).

composition $Sr_{0.7}Ba_{1.2}Eu_{0.05}Li_{0.05}CaWO_6$, if the emission wavelength monitored is 615 nm, the CT band (due to WO_6 octahedra) is low and the sharp lines at 465 and 545 nm are high (due to Eu^{3+} levels) (Fig. 11). On the other hand, when the emission wavelength

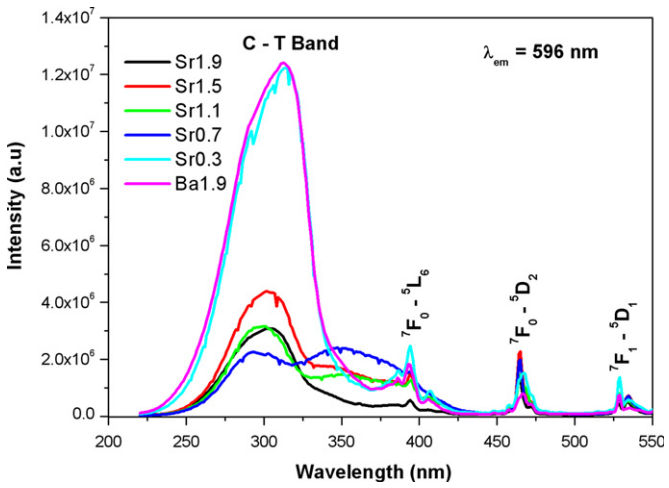

Fig. 12. PL excitation spectra of select compositions $Sr_{1.9-x}Ba_xEu_{0.05}Li_{0.05}CaWO_6$ ($x = 0$–1.9; $\lambda_{em} = 596$ nm).

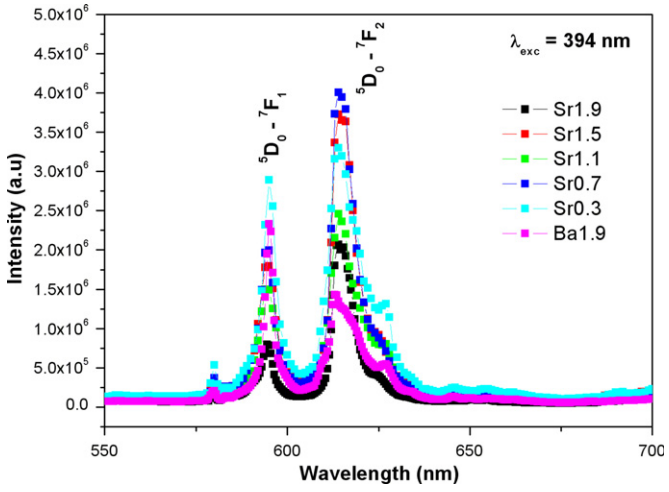

Fig. 13. PL emission spectra of select compositions $Sr_{1.9-x}Ba_xEu_{0.05}Li_{0.05}CaWO_6$ ($x = 0$–1.9; $\lambda_{exc} = 394$ nm).

monitored is 596 nm (Fig. 12), the intensity of the CT band is very high compared to that of the *f*–*f* transitions of Eu^{3+} for all compositions.

The emission spectra of select compositions $Sr_{1.9-x}Ba_xEu_{0.05}Li_{0.05}CaWO_6$ ($x = 0$–1.9, in steps of 0.2) are shown in Fig. 13. Eu^{3+}-substituted phases show two emission lines at around 596 nm (MD) and 615 nm (ED); however, the relative emission intensity of ED and MD transitions and splitting of the emission lines depends on the Ba content in the lattice. These emission lines are observed ($^5D_0$–$^7F_1$ and $^5D_0$–$^7F_2$) under either CT band (due to WO_6 octahedra) or 395/465 nm (due to *f*–*f* transition of Eu^{3+}) excitation. Fig. 14 shows the relative emission intensity of ED and MD transitions versus Ba content. If the Ba content is less in the lattice ($x \leqslant 1.2$), orange-red emission is observed (MD and ED), whereas intense orange emission (MD) is observed for $x \geqslant 1.8$. It has been reported that in the cubic structure *B*–O–*B*′ bond is linear, whereas, in lower symmetry structures the *B*–O–*B*′ angle distorts away from 180° and the *A*-site coordination polyhedron becomes distorted [9]. The presently studied compound Sr_2CaWO_6 crystallizes in monoclinic structure. Hence, one can expect *A*-site distortion and when the Eu^{3+} occupies *A*-site, it shows both orange (596 nm, MD) and red (615 nm, ED) emission.

This result clearly reveals that the *A*-site coordination polyhedron is distorted and the inversion symmetry is no longer

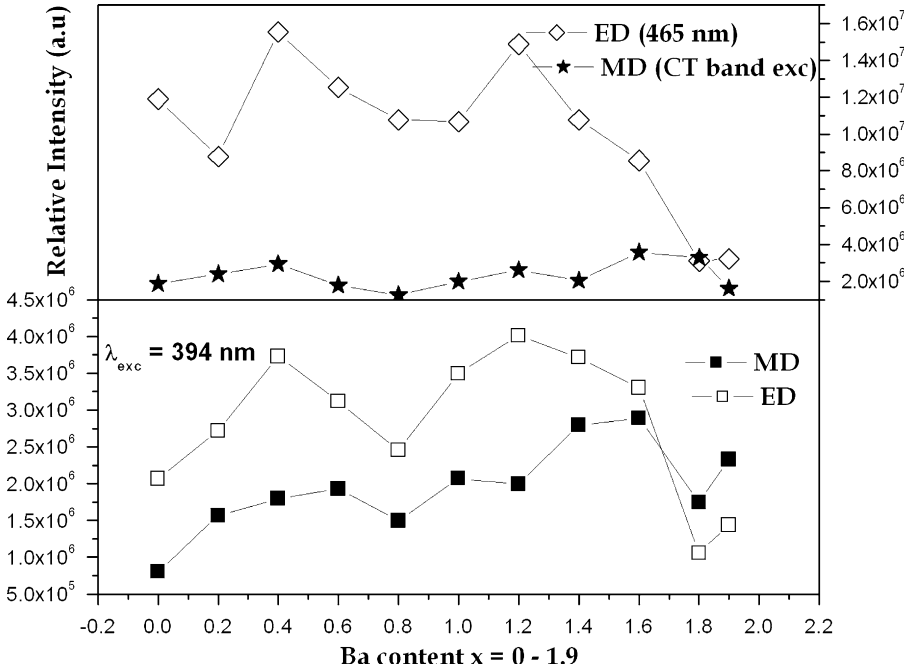

Fig. 14. Relative emission intensity of MD and ED transitions of $Sr_{1.9-x}Ba_xEu_{0.05}Li_{0.05}CaWO_6$ ($x = 0$–1.9, in steps of 0.2).

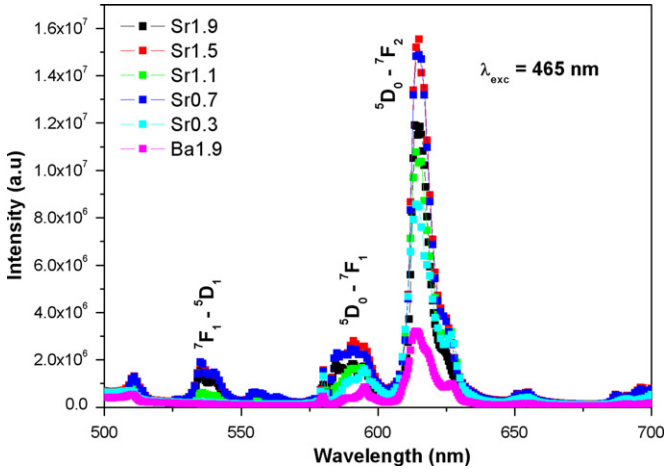

Fig. 15. PL emission spectra of select compositions $Sr_{1.9-x}Ba_xEu_{0.05}Li_{0.05}CaWO_6$ ($x = 0$–1.9; $\lambda_{exc} = 465$ nm).

present. Similar observation has been documented for Eu^{3+} ion-substituted (*A*-site) orthorhombically distorted perovskite compound $GdAlO_3$ [19,20]. As mentioned earlier, Ba_2CaWO_6 crystallizes in the pseudo-cubic structure and both *A*- and *B*-sites polyhedra are not distorted. Accordingly the MD transition is stronger in the emission spectra (Fig. 13). These results reveal that crystal chemistry plays an important role in determining the luminescence property. The emission intensity is found to be highest for the compositions $Sr_{1.5}Ba_{0.4}Eu_{0.05}Li_{0.05}CaWO_6$ and $Sr_{0.3}Ba_{1.6}Eu_{0.05}Li_{0.05}CaWO_6$ with red and orange emission, respectively ($\lambda_{exc} = 394$ nm). However, remarkably, all Eu^{3+}-substituted compositions show forced ED transition (red emission) under 465 nm excitation (Fig. 15). The intensity of the ED is found to be high for the composition $Sr_{1.5}Eu_{0.05}Li_{0.05}Ba_{0.4}CaWO_6$. The intensity of $^5D_0 \rightarrow {}^7F_2$ emission line of all compositions is compared with that of the $Y_2O_2S{:}Eu^{3+}$ commercial red phosphor (Nichia) and the relative emission intensity of $Sr_{1.5}Eu_{0.05}Li_{0.05}Ba_{0.4}CaWO_6$ composition is found to be ~4.5 times higher than that of commercial one under 465 nm excitation.

4. Conclusions

The photoluminescence studies have been carried out for Eu^{3+}-substituted (both *A*- and *B*-sites) A_2CaWO_6 (A = Sr, Ba) phosphor and the results reveal that the *A*-site-substituted compositions show both ED and MD transitions for Sr analogue composition, whereas only intense MD transitions are found for Ba analogue compositions. The results are consistent with the crystal structure. In $Sr_{1.9-x}Ba_xEu_{0.05}Li_{0.05}CaWO_6$ ($x = 0$–1.9, in steps of 0.2), compositionally induced phase transition has been observed from monoclinic to pseudo-cubic structure for $x \leqslant 0.2$. The MD and ED transitions are found for all compositions (under CT band/394 nm); however, the relative emission intensity depends on the Ba content present in the host lattice. Noticeably, all the compositions show dominant ED transition under blue ray excitation (465 nm). The red emission of $Sr_{1.5}Eu_{0.05}Li_{0.05}Ba_{0.4}CaWO_6$ is found to be ~4.5 times higher than that of commercial red phosphor (Nichia) under 465 nm excitation and hence this phosphor could be a potential candidate for white LED based on blue GaN LED.

Acknowledgment

The author V.S.K. acknowledges the Council of Scientific and Industrial Research (CSIR), New Delhi for research fellowship.

References

[1] S. Nakamura, T. Mukai, M. Senoh, J. Appl. Phys. 76 (1994) 8189.
[2] R. Muller-Mach, G.O. Mueller, IEEE J. Sel. Top. Quantum Electron. 8 (2002) 339.
[3] A.M. Srivastava, H.A. Comanzo, US Patent 6501, 2002, 100pp.
[4] T. Taguchi, OE Mag. 3 (2003) 13.
[5] V. Sivakumar, U.V. Varadaraju, J. Electrochem. Soc. 152 (2005) H168.
[6] V. Sivakumar, U.V. Varadaraju, J. Electrochem. Soc. 153 (2006) H54.
[7] V. Sivakumar, U.V. Varadaraju, Electrochem. Solid State Lett. 9 (2006) H35.
[8] V. Sivakumar, U.V. Varadaraju, J. Electrochem. Soc. 154 (2007) J28.
[9] M.T. Anderson, K.B. Greenwood, G.A. Taylor, K.R. Poeppelmeier, Prog. Solid State Chem. 22 (3) (1993) 197.
[10] E.G. Steward, H.P. Rooksby, Acta Crystallogr. 4 (1951) 503.

[11] M. Gateshki, J.M. Igartua, J. Phys.: Condens. Matter 16 (37) (2004) 6639.
[12] M.W. Lufaso, P.W. Barnes, P.M. Woodward, Acta Crystallogr. B 62 (2006) 397.
[13] V. Sivakumar, Investigation of rare earth luminescence in mixed metal oxides and silicates, Ph.D Thesis, IIT Madras, India, 2007.
[14] G. Blasse, J. Inorg. Nucl. Chem. 27 (1965) 993.
[15] R.D. Shannon, C.T. Prewitt, Acta Crystallogr. B 25 (1969) 925.
[16] H.W. Eng, P.W. Barnes, B.M. Auer, P.M. Woodward, J. Solid State Chem. 175 (2003) 94.
[17] L.I. Katzin, Inorg. Chem. 8 (1969) 1649.
[18] G. Blasse, B.C. Grabmaier, Luminescent Materials, Springer, Berlin, 1994.
[19] M.J. Weber, R.F. Schaufele, Phys. Rev. 138 (1965) A1544.
[20] G. Blasse, A. Bril, W.C. Nieuwpoort, J. Phys. Chem. Solids 27 (1966) 1587.
[21] J.H.G. Bode, A.B. Van oosterhout, J. Lumin. 10 (1975) 237.